Available online at www.sciencedirect.com
SCIENCE DIRECT®
International Journal of Solids and Structures 42 (2005) 4588–4612
INTERNATIONAL JOURNAL OF SOLIDS and STRUCTURES
www.elsevier.com/locate/ijsolstr

An embedding method for modeling micromechanical behavior and macroscopic properties of composite materials

J. Wang [a,*], S.G. Mogilevskaya [b], S.L. Crouch [b]

[a] Department of Civil and Coastal Engineering, University of Florida, 365 Weil Hall, P.O. Box 116580, Gainesville, FL 32611, USA
[b] Department of Civil Engineering, University of Minnesota, 500 Pillsbury Drive S.E., Minneapolis, MN 55455, USA

Received 29 September 2004; received in revised form 8 February 2005
Available online 19 March 2005

Abstract

This paper presents a numerical method for modeling the micromechanical behavior and macroscopic properties of fiber-reinforced composites and perforated materials. The material is modeled by a finite rectangular domain containing multiple circular holes and elastic inclusions. The rectangular domain is assumed to be embedded within a larger circular domain with fictitious boundary loading represented by truncated Fourier series. The analytical solution for the complementary problem of a circular domain containing holes and inclusions is obtained by using a combination of the series expansion technique with a direct boundary integral method. The boundary conditions on the physical external boundary are satisfied by adopting an overspecification technique based on a least squares approximation. All of the integrals arising in the method can be evaluated analytically. As a result, the elastic fields and effective properties can be expressed explicitly in terms of the coefficients in the series expansions. Several numerical experiments are conducted to verify the accuracy and efficiency of the numerical method and to demonstrate its application in determination of the macroscopic properties of composite materials.

Keywords: Embedding method; Fiber-reinforced composites; Perforated materials; Effective properties; Direct boundary integral method; Fourier series; Least squares

* Corresponding author. Tel.: +1 352 392 9537; fax: +1 352 392 3394.
E-mail address: jwang@ce.ufl.edu (J. Wang).

0020-7683/$ - see front matter © 2005 Elsevier Ltd. All rights reserved.
doi:10.1016/j.ijsolstr.2005.02.006

1. Introduction

Fiber-reinforced composites and perforated materials are widely used in engineering structures. Some of these materials (for example, unidirectional fiber-reinforced composites, or thin-plate solids consisting of disks or holes) can be represented as two-dimensional linearly elastic solids containing multiple holes and locally isotropic inclusions. The inclusions refer to the fibers or disks in composite materials and the holes are either due to the inherent porosity of the material or a result of the manufacturing process (i.e. caused by drilling). The holes and inclusions cause significant stress disturbance, especially when they are closely spaced, leading to a considerable change of the macroscopic properties as well as the micromechanical behavior of the material. Thus, it is of engineering importance to calculate the elastic fields and effective properties of a two-dimensional solid containing multiple holes and inclusions. In the work presented in this paper, we consider the particular but practically important case in which the holes and inclusions are circular.

This paper presents an extension of the previous work of the authors on modeling composite materials using a direct boundary integral approach, which was first presented by Mogilevskaya and Crouch (2001) for multiple circular inclusions in an infinite plane. This approach was later extended to include circular holes as well as cracks (e.g. Wang et al., 2001, 2003a,c) and to consider a finite domain with a circular boundary (Wang et al., 2003c). These analyses combine the series expansion technique with a direct boundary integral method in which complex singular and hypersingular integrals are written directly in terms of the actual boundary tractions, displacements, and—for cracks—displacement discontinuities (Linkov and Mogilevskaya, 1994). The unknown boundary parameters are expressed globally in terms of series expansions of orthogonal functions (i.e. Fourier series for circular boundaries and Chebyshev polynomials for cracks). All the integrals involved in the analyses are evaluated analytically and numerical errors only come from truncation of the series. After incorporating a fast multipole algorithm, the approach is capable of solving large scale practical problems involving thousands of objects (e.g. Wang et al., in press). Because of its analytic nature, the approach has advantages in accuracy and efficiency over some other numerical methods [for example, the series expansion method (Isida and Sato, 1984; Wang et al., 2000), the finite element method (Meguid, 1986; Wacker et al., 1998), and the standard boundary element method (Eischen and Torquato, 1993; Greengard and Helsing, 1998; Liu et al., 2000; Kong et al., 2002)] for the particular problem under consideration.

In this paper, we consider a finite domain of rectangular or square shape. Such a model can be used to design laboratory experiments for direct measurement of micromechanical behavior and macroscopic properties of composite materials. For a domain of such shape, however, the problem can no longer be solved analytically. In order to retain the main features of our approach, we suggest a simple embedding technique that is well tailored for this particular type of problem. Instead of solving the problem directly, we embed the physical solution domain into a circular disc and apply fictitious loading on the boundary so as to satisfy the prescribed conditions on the physical external boundary. The subsequent analysis is based on the analytical solution we have obtained for multiple circular inclusions and holes in a finite circular domain (Wang et al., 2003c).

The term "embedding method" is used in the literature to describe different numerical techniques, all of which consider the physical solution domain as a part of a larger fictitious domain with simple geometry. In one of these approaches by Boley and collaborators (Boley, 1961; Boley and Yagoda, 1971), the fictitious boundary conditions on the artificial boundary are found by satisfying the conditions on the real physical boundary. In our approach, we use the term "embedding method" in the same sense as Boley (1961) and Boley and Yagoda (1971) with the embedding domain chosen to be circular. Following Wang et al. (2003c), the fictitious tractions and displacements on the boundary of the embedding domain and other unknown boundary functions are approximated by truncated complex Fourier series. As a result, all the integrals involved in the analysis are evaluated analytically. The stress and displacement fields everywhere inside the

circular domain can be expressed explicitly in terms of analytic functions of the coefficients in the series expansions. The boundary conditions for the inclusions and holes are satisfied analytically, and for the actual external boundary are satisfied by adopting an overspecification technique based on a least squares approximation. An iterative algorithm is developed to implement the numerical scheme outlined above. Convergence of the algorithm is independent of the initial choice of the fictitious tractions and displacements. Global approximation of the boundary parameters without boundary discretization and analytical evaluation of all the integrals yields high accuracy of the numerical results with relatively low computational cost.

In the succeeding sections of this paper, we give the theoretical formulation of the embedding technique applied to problems of multiple circular holes and elastic inclusions in a finite rectangular domain, as well as its numerical implementation using the solution obtained for the counterpart of the subject problem in a circular domain. An iterative algorithm is described to obtain the numerical solution. Several numerical experiments are described to verify the accuracy and effectiveness of the method and to demonstrate its application in determining the effective properties of fiber-reinforced composites. Finally, some concluding remarks are made regarding the advantages and possible extensions of the work.

2. Problem statement

We consider a linearly elastic finite rectangular domain $\mathscr{D}$ containing an arbitrary assortment nonoverlapping circular holes and elastic inclusions (Fig. 1). The inclusions are assumed to be perfectly bonded with the matrix, although this restriction can easily be relaxed by incorporating spring-type interface conditions (Mogilevskaya and Crouch, 2002) or adding an interphase layer (Mogilevskaya and Crouch, 2004). The holes are either traction free or loaded with uniformly distributed normal pressure. The entire region is subjected to arbitrary (but equilibrated) loading on the external boundary Γ_e.

The numbers of inclusions and holes inside the domain are N_p and N_h, respectively. The elastic properties of the inclusions (shear moduli μ_j^p and Poisson's ratios $\nu_j^p, j = 1, \ldots, N_p$) are arbitrary, and different from the elastic constants of the matrix μ_m and ν_m. Let R_j^p, z_j^p, and Γ_j^p denote the radius, center, and boundary of the jth inclusion; let R_j^h, z_j^h, and Γ_j^h denote these same quantities for the jth hole; and let p_j denote the constant normal traction acting on Γ_j^h ($p_j < 0$ for compression). The regions enclosed by contours Γ_j^p and Γ_j^h are denoted by $\mathscr{D}_j^p$ and $\mathscr{D}_j^h$, respectively. We define the following unions

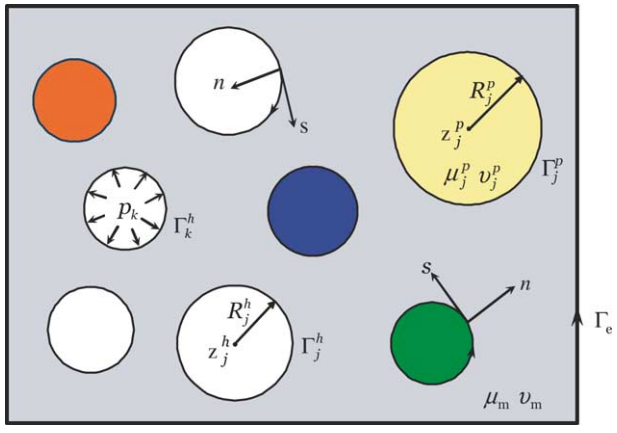

Fig. 1. Multiple circular holes and inclusions in a finite rectangular domain.

$$\Gamma^p = \bigcup_{j=1}^{N_p} \Gamma_j^p, \quad \Gamma^h = \bigcup_{j=1}^{N_h} \Gamma_j^h \quad \text{and} \quad \mathscr{D}^p = \bigcup_{j=1}^{N_p} \mathscr{D}_j^p, \quad \mathscr{D}^h = \bigcup_{j=1}^{N_h} \mathscr{D}_j^h. \tag{1}$$

The direction of travel is clockwise for holes Γ_j^h ($j = 1, \ldots, N_h$), and counter-clockwise for inclusions Γ_j^p ($j = 1, \ldots, N_p$) and the finite external boundary Γ_e. The unit tangent s points in the direction of travel and the unit outward normal n points to the right of this direction. Any point in the domain is identified by the complex coordinate $z = x + iy$ ($i = \sqrt{-1}$). The stresses and displacements in the finite region are to be determined.

3. Theoretical formulation

3.1. Potential representation

The displacements and stresses at any point z inside the solution domain can be calculated using the Kolosov–Muskhelishvili formulae (Muskhelishvili, 1963), which are expressed in terms of two analytic functions $\varphi(z)$ and $\psi(z)$ as follows:

$$\begin{aligned} u_x(z) + iu_y(z) &= \frac{1}{2\mu}\left[\kappa\varphi(z) - z\overline{\varphi'(z)} - \overline{\psi(z)}\right], \\ \sigma_{xx} + \sigma_{yy} &= 4\mathrm{Re}\,\varphi'(z), \\ \sigma_{yy} - \sigma_{xx} + 2i\sigma_{xy} &= 2[\bar{z}\varphi''(z) + \psi'(z)]. \end{aligned} \tag{2}$$

In these equations, Muskhelishvili's parameter κ is $3 - 4\nu$ for plane strain and $(3 - \nu)/(1 + \nu)$ for plane stress; μ and ν are the shear modulus and Poisson's ratio; $u_x(z)$ and $u_y(z)$ are the displacements; and σ_{xx}, σ_{yy}, and σ_{xy} are the components of the stress tensor.

The Kolosov–Muskhelishvili potentials $\varphi(z)$ and $\psi(z)$ for more general problems of a finite or infinite plane containing inclusions, holes, and cracks of arbitrary shapes have been obtained in (Linkov and Mogilevskaya, 1998) using a superposition procedure described by Linkov (1983). They can be written in terms of the physical boundary parameters (i.e. boundary tractions, displacements, and displacement discontinuities) in the form of integral expressions as:

$$\begin{aligned} \varphi(z) &= -\eta[\Lambda_1\sigma(z) - \Lambda_2\Delta u(z)], \\ \psi(z) &= -\eta[\Lambda_3\sigma(z) + \Lambda_4\Delta u(z)], \end{aligned} \tag{3}$$

where η is a constant defined as

$$\eta = \frac{2\mu}{\kappa + 1} \quad \text{and} \quad \begin{cases} \mu = \mu_j^p, \kappa = \kappa_j^p, z \in \mathscr{D}_j^p; \\ \mu = \mu_m, \kappa = \kappa_m, z \in \mathscr{D} - (\mathscr{D}^p \cup \mathscr{D}^h) \end{cases} \tag{4}$$

and the integral operators Λ_k ($k = 1, \ldots, 4$) acting on function $f(z)$ are given by

$$\begin{aligned} \Lambda_1 f(z) &= \frac{1}{2\pi i}\int_\Gamma a_1 f(\tau)\ln(\tau - z)\,d\tau, \\ \Lambda_2 f(z) &= \frac{1}{2\pi i}\int_\Gamma \frac{f(\tau)}{\tau - z}\,d\tau, \\ \Lambda_3 f(z) &= \frac{1}{2\pi i}\left[\int_\Gamma a_1\frac{f(\tau)}{\tau - z}\bar{\tau}\,d\tau - \int_\Gamma (a_1 - a_3)\overline{f(\tau)}\ln(\tau - z)\,d\bar{\tau}\right], \\ \Lambda_4 f(z) &= \frac{1}{2\pi i}\left[\int_\Gamma \frac{\overline{f(\tau)}}{\tau - z}\,d\tau - \int_\Gamma \frac{f(\tau)}{\tau - z}\,d\bar{\tau} + \int_\Gamma \frac{f(\tau)}{(\tau - z)^2}\bar{\tau}\,d\tau\right], \end{aligned} \tag{5}$$

where Γ is the union of all boundaries (in our case $\Gamma = \Gamma_e \cup \Gamma^p \cup \Gamma^h$); $\sigma = \sigma_n + i\sigma_s$ is the complex-valued boundary traction (in the local coordinate system), with normal and shear components σ_n and σ_s; $\Delta u = u^+ - u^-$ is the complex-valued displacement discontinuity, and $u^\pm = u_x^\pm + iu_y^\pm$ are the limit values of the displacements (in the global coordinate system) when the contour is approached from its left and right sides, respectively. For a finite domain containing only holes and perfectly bonded inclusions, we have

$$\Delta u(z) = \begin{cases} 0, & z \in \Gamma^p, \\ u(z), & z \in \Gamma_e \cup \Gamma^h. \end{cases} \tag{6}$$

The real-valued constants a_1 and a_3 are combinations of elastic constants from different sides of the boundaries and, for each individual inclusion j, are defined as

$$a_{1j} = \frac{1}{2\mu_j^p} - \frac{1}{2\mu_m}; \quad a_{3j} = \frac{1+\kappa_j^p}{2\mu_j^p} - \frac{1+\kappa_m}{2\mu_m}. \tag{7}$$

For holes and the finite boundary, they are

$$a_1 = \frac{1}{2\mu_m}; \quad a_3 = \frac{1+\kappa_m}{2\mu_m}. \tag{8}$$

Based on the principle of superposition, each individual integral operator Λ_k ($k = 1, \ldots, 4$) in (5) is decomposed into two operators $\Lambda_k^{(i)}$ and $\Lambda_k^{(e)}$ as

$$\Lambda_k f(z) = \left(\Lambda_k^{(i)} + \Lambda_k^{(e)}\right) f(z), \quad (k = 1, \ldots, 4), \tag{9}$$

where $\Lambda_k^{(i)}$ is defined over all internal boundaries $\Gamma_i = \Gamma^p \cup \Gamma^h$ and $\Lambda_j^{(e)}$ is defined over the external boundary Γ_e; $\Lambda_k^{(i)}$ can be further decomposed as

$$\Lambda_k^{(i)} f(z) = \left(\sum_{j=1}^{N_p} \Lambda_{kj}^p + \sum_{j=1}^{N_h} \Lambda_{kj}^h \right) f(z), \quad (k = 1, \ldots, 4) \tag{10}$$

with Λ_{kj}^p and Λ_{kj}^h defined over Γ_j^p and Γ_j^h, respectively.

After substituting (9) and (10) into (5) and (3), the potentials $\varphi(z)$ and $\psi(z)$ can be written as a superposition of the potentials for the individual internal boundaries (the individual holes and the individual inclusions) and the potentials arising from the conditions on the external boundary,

$$\begin{aligned} &\varphi(z) = \varphi^{(i)}(z) + \varphi^{(e)}(z) \quad \text{and} \quad \varphi^{(i)}(z) = \sum_{j=1}^{N_p} \varphi_j^p(z) + \sum_{j=1}^{N_h} \varphi_j^h(z), \\ &\psi(z) = \psi^{(i)}(z) + \psi^{(e)}(z) \quad \text{and} \quad \psi^{(i)}(z) = \sum_{j=1}^{N_p} \psi_j^p(z) + \sum_{j=1}^{N_h} \psi_j^h(z), \end{aligned} \tag{11}$$

where

$$\begin{aligned} &\varphi^{(e)}(z) = -\eta[\Lambda_1^{(e)}\sigma(z) - \Lambda_2^{(e)}u(z)], \quad \psi^{(e)}(z) = -\eta[\Lambda_3^{(e)}\sigma(z) + \Lambda_4^{(e)}u(z)], \\ &\varphi_j^p(z) = -\eta\Lambda_{1j}^p\sigma(z), \quad \psi_j^p(z) = -\eta\Lambda_{3j}^p\sigma(z), \\ &\varphi_j^h(z) = -\eta[\Lambda_{1j}^h p_j - \Lambda_{2j}^h u(z)], \quad \psi_j^h(z) = -\eta[\Lambda_{3j}^h p_j + \Lambda_{4j}^h u(z)]. \end{aligned} \tag{12}$$

Notice that in simplifying the above expressions, we have used condition (6) and the assumption that Γ_j^h is loaded with constant normal traction p_j.

3.2. An embedding method

The idea of this method can be explained from both physical and mathematical points of view. Physically, we suppose that the original finite region containing the circular inclusions and holes is embedded into a larger domain whose boundary conditions are fictitious and are constructed such that the physical conditions prescribed on the boundary of the original domain are satisfied. In our work, the larger fictitious domain is chosen to be a circular region with center z_o, radius R_o, and boundary Γ_o, as shown in Fig. 2. If the fictitious boundary conditions applied on Γ_o can be defined in such a way that the boundary conditions prescribed on Γ_e are satisfied, then, because solutions to linear elasticity problems are unique, the original problem with the physical boundary Γ_e is solved as well.

Mathematically, the procedure means that the analytical functions $\varphi^{(o)}(z)$ and $\psi^{(o)}(z)$ that solve the problem in the larger circular domain are analytic continuations of the Kolosov-Muskhelishvili potentials for the problem in the original physical domain. The question of existence of embedding solutions for the general case of a finite domain with general types of boundary conditions requires further investigation. In the present paper, we verify by means of examples that the embedding method works well for problems where the domain $\mathscr{D}$ is square or rectangular.

The potentials $\varphi^{(o)}(z)$ and $\psi^{(o)}(z)$ for a general problem are not known but can be found from the numerical procedure described in the next section. In the new formulation, after embedding a finite domain containing multiple holes and elastic inclusions into a fictitious circular domain, the external boundary Γ_e is replaced by the pseudo circle Γ_o, on which the fictitious boundary conditions are assumed to be prescribed and expanded into complex Fourier series. Accordingly, the integral operators $\Lambda_k^{(e)}$ defined over Γ_e and the corresponding potentials $\varphi^{(e)}(z)$ and $\psi^{(e)}(z)$ in (9)–(12) are not present, but are replaced by their counterparts defined on Γ_o,

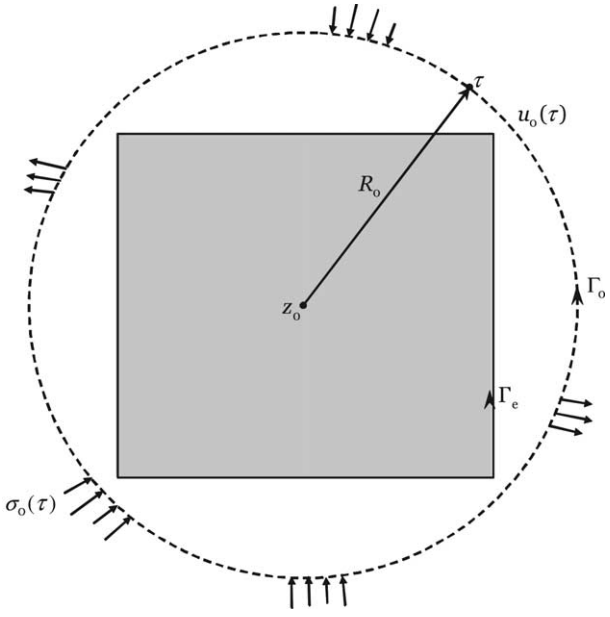

Fig. 2. A rectangular physical domain embedded within a fictitious circular domain.

$$\begin{aligned} &\Lambda_k^{(e)} \to \Lambda_k^{(o)}, \quad (k = 1, \ldots, 4), \\ &\varphi^{(e)}(z), \quad \psi^{(e)}(z) \to \varphi^{(o)}(z), \quad \psi^{(o)}(z), \end{aligned} \tag{13}$$

where the integral operators $\Lambda_k^{(o)}$ act on the fictitious tractions and displacements, denoted by $\sigma_o(\tau)$ and $u_o(\tau)$ at $\tau \in \Gamma_o$, respectively.

The displacement and stress fields inside the fictitious domain enclosed by Γ_o are obtained by substituting the expressions for the potentials into the Kolosov–Muskhelishvili formulae (2). The tractions $t(z) = t_x(z) + \mathrm{i}t_y(z)$ in the global coordinate system and $\sigma(z) = \sigma_n(z) + \mathrm{i}\sigma_s(z)$ in the local coordinate system along a curve χ are calculated based on the components of the stress tensor,

$$t(z) = n(z)S_m(z) - \overline{n(z)S_d(z)}, \tag{14}$$

$$\sigma(z) = S_m(z) + \frac{\mathrm{d}\bar{z}}{\mathrm{d}z}\overline{S_d(z)}, \tag{15}$$

where $S_m(z)$ and $S_d(z)$ are defined as

$$S_m(z) = \frac{\sigma_{xx}(z) + \sigma_{yy}(z)}{2}, \quad S_d(z) = \frac{\sigma_{yy}(z) - \sigma_{xx}(z)}{2} + \mathrm{i}\sigma_{xy}(z) \tag{16}$$

and where $n(z) = n_x(z) + \mathrm{i}n_y(z)$ is the unit outward normal at point z on χ, $\mathrm{d}\bar{z}/\mathrm{d}z = \exp(-2\mathrm{i}\beta)$ and β is the angle between the tangent to curve χ at point z and the positive x-axis. In this paper, we use $\sigma(z)$ for all circular boundaries (including all internal boundaries Γ_i and the pseudo circular boundary Γ_o), and $t(z)$ for the physical external boundary Γ_e.

Now suppose that the solution is obtained for a problem in the fictitious circular domain with initial loading over the external boundary Γ_o represented by truncated complex Fourier series. The displacements $u(z)$ and tractions $t(z)$ at any point z on the physical external boundary Γ_e are found in terms of the Fourier coefficients from the solution of the elastic fields and the relationship expressed in (14) and (16). The original problem is solved if and only if the boundary displacements and tractions over Γ_e meet the prescribed displacements u^{pr} and tractions t^{pr}:

$$t^{pr}(z) = t_x^{pr}(z) + \mathrm{i}t_y^{pr}(z), \quad z \in \Gamma_e^{(t)}, \tag{17}$$

$$u^{pr}(z) = u_x^{pr}(z) + \mathrm{i}u_y^{pr}(z), \quad z \in \Gamma_e^{(u)}, \tag{18}$$

where $\Gamma_e^{(t)}$ and $\Gamma_e^{(u)}$ denote the parts of Γ_e where tractions and displacements are prescribed, respectively, and $\Gamma_e^{(t)} \cup \Gamma_e^{(u)} = \Gamma_e$. Thus, the initial fictitious loading over the pseudo boundary Γ_o must be adjusted to satisfy the boundary conditions over the physical boundary Γ_e.

The coefficients in the Fourier expansion can be computed by adopting an overspecification technique, the principle of which is to meet the boundary conditions approximately in an average sense (e.g. using least squares) using a larger set of control points rather than meeting the conditions exactly at specific points, as adopted in the collocation method (Barnes and Janković, 1999). As a result, a new set of coefficients is obtained by solving the following least squares problem:

$$\min\left\{\int_{\Gamma_e^{(t)}}[t(z) - t^{pr}(z)]^2\mathrm{d}z + \int_{\Gamma_e^{(u)}}[u(z) - u^{pr}(z)]^2\mathrm{d}z\right\}. \tag{19}$$

The integral representation of least squares (19) gives the best approximation of the boundary conditions in the mean. In order to avoid integrations over the finite external boundary Γ_e, we apply the discrete least squares condition:

$$\min\left\{\sum_{k=1}^{M_c^t}\left[t(z_k)-t^{pr}(z_k)\right]^2\Big|_{z_k\in\Gamma_e^{(t)}}+\sum_{k=1}^{M_c^u}\left[u(z_k)-u^{pr}(z_k)\right]^2\Big|_{z_k\in\Gamma_e^{(u)}}\right\}, \tag{20}$$

where M_c^t and M_c^u are the numbers of control points over $\Gamma_e^{(t)}$ and $\Gamma_e^{(u)}$, respectively. An algorithm based on QR decomposition (Golub and Van Loan, 1996) is used in this paper to solve the least squares problem described in (20).

4. Numerical implementation of the embedding method

In the following discussion, we describe in detail the procedure for implementing the embedding method for the problem of interacting circular holes and elastic inclusions. We first review the solution obtained by Wang et al. (2003c) for the same problem in a finite circular domain. Based on this solution and the concept of embedding, an iterative algorithm is developed in combination with an overspecification technique to solve the problem in a general finite convex domain.

4.1. Complex Fourier series representation

Following Wang et al. (2003c), we use series expansions to approximate the fictitious tractions and displacements on the pseudo circular boundary Γ_o and all other unknown physical boundary functions, including the unknown tractions on the boundaries of the inclusions and the unknown displacements on the boundaries of the holes. For notational convenience, we define the following functions

$$f_o(\tau)=\frac{R_o}{\tau-z_o},\quad f_{pj}(\tau)=\frac{R_j^p}{\tau-z_j^p},\quad \text{and}\quad f_{hj}(\tau)=\frac{R_j^h}{\tau-z_j^h}. \tag{21}$$

We expand the fictitious tractions $\sigma_o(\tau)$ and displacements $u_o(\tau)$ on Γ_o into truncated complex Fourier series as

$$\sigma_o(\tau)=b_{0o}+\sum_{m=1}^{M_o}\left[b_{-mo}f_o^m(\tau)+b_{mo}f_o^{-m}(\tau)\right],\quad \tau\in\Gamma_o, \tag{22}$$

$$u_o(\tau)=c_{0o}+\sum_{m=1}^{M_o}\left[c_{-mo}f_o^m(\tau)+c_{mo}f_o^{-m}(\tau)\right],\quad \tau\in\Gamma_o. \tag{23}$$

Similarly, the unknown tractions $\sigma_j^p(\tau)$ on the boundaries Γ_j^p of the inclusions and the unknown displacements $u_j^h(\tau)$ on the boundaries Γ_j^h of the holes are also approximated by truncated complex Fourier series,

$$\sigma_j^p(\tau)=b_{0j}+\sum_{m=1}^{M_{pj}}\left[b_{-mj}f_{pj}^m(\tau)+b_{mj}f_{pj}^{-m}(\tau)\right],\quad \tau\in\Gamma_j^p, \tag{24}$$

$$u_j^h(\tau)=c_{0j}+\sum_{m=1}^{M_{hj}}\left[c_{-mj}f_{hj}^m(\tau)+c_{mj}f_{hj}^{-m}(\tau)\right],\quad \tau\in\Gamma_j^h. \tag{25}$$

No assumptions are made regarding the numbers of terms in the above series—the values of M_o, M_{pj}, and M_{hj} must be selected for any particular problem, but are arbitrary. The determination of these numbers will be discussed later.

Suppose we have an initial distribution of fictitious tractions $\sigma_o(\tau)$ on Γ_o with known coefficients b_{0o} and $b_{\pm mo}$ $(m = 1, \ldots, M_o)$ in expansion (22). All the other complex coefficients c_{0o} and $c_{\pm mo}$ $(m = 1, \ldots, M_o)$, b_{0j} and $b_{\pm mj}$ $(m = 1, \ldots, M_{pj})$, c_{0j} and $c_{\pm mj}$ $(m = 1, \ldots, M_{hj})$ involved in the above series expansions then need to be determined. By equilibrium (i.e. the resultant force and moment on the pseudo boundary and the individual holes and inclusions are equal to zero), we have

$$b_{-1o} = b_{-1j} = 0 \quad \text{and} \quad b_{0o}, b_{0j} \text{ are real.} \tag{26}$$

4.2. Expressions for stresses and displacements

Based on the above global representations of the boundary tractions and displacements, all of the integrals involved in (12) with the replacement condition (13) incorporated can be calculated analytically by using the Cauchy integral theorem or the residue theorem for the individual closed contours. The details and the corresponding results for evaluating the integral operators $\Lambda_k^{(o)}\sigma(z)$, $\Lambda_{kj}^{p}\sigma(z)$, $\Lambda_{kj}^{h}p_j$ $(k = 1, 3)$, and $\Lambda_k^{(o)}u(z)$, $\Lambda_{kj}^{h}u(z)$ $(k = 2, 4)$ are given in Wang et al. (2003c). As a result, we obtain the explicit expressions for the potentials recorded in Appendix A.

Substituting the expressions (A.1)–(A.6) into (11) and then the resulting expressions for potentials $\varphi(z)$ and $\psi(z)$ into the Kolosov–Muskhelishvili formulae (2), we obtain analytic expressions for the displacements and stresses in terms of the coefficients in the series expansions (22)–(25). The latter expressions are given as a superposition of contributions from each individual boundary. The displacements at point z are given as

$$u(z) = u^{(i)}(z) + u^{(o)}(z) \quad \text{and} \quad u^{(i)}(z) = \sum_{j=1}^{N_p} u_j^p(z) + \sum_{j=1}^{N_h} u_j^h(z) \tag{27}$$

with the individual terms $u^{(o)}(z)$, $u_j^p(z)$, and $u_j^h(z)$ corresponding to contributions from the pseudo circular boundary, the individual inclusions, and the individual holes, respectively. Similarly, the expressions for the stress components $S_m(z)$ and $S_d(z)$ at point z are given as

$$S_*(z) = S_*^{(i)}(z) + S_*^{(o)}(z) \quad \text{and} \quad S_*^{(i)}(z) = \sum_{j=1}^{N_p} S_{*j}^p(z) + \sum_{j=1}^{N_h} S_{*j}^h(z), \quad (* = m, d). \tag{28}$$

4.3. A linear algebraic system

Letting point z approach each individual boundary, we obtain boundary values of the displacements from expression (27). According to the conditions expressed in (6), the displacements are continuous across the boundary of each inclusion Γ_k^p,

$$u(z)|_{z\to\Gamma_k^{p+}} = u(z)|_{z\to\Gamma_k^{p-}}, \quad (k = 1, \ldots, N_p) \tag{29}$$

and the traction obtained by substituting (28) into (15) for the boundary points on Γ_k^h and Γ_o should equal the prescribed values, that is

$$\sigma(z)|_{z\to\Gamma_k^{h+}} = p_k, \quad (k = 1, \ldots, N_h), \tag{30}$$

$$\sigma(z)|_{z\to\Gamma_o^{+}} = \sigma_o(z) = \left\{ b_{0o} + \sum_{m=1}^{M_o} [b_{-mo} f_o^m(z) + b_{mo} f_o^{-m}(z)] \right\}_{z\in\Gamma_o}. \tag{31}$$

The superscript +(−) in the above equations indicates that point z approaches the boundary from the left (right) side with respect to the direction of travel. The functions expressed in (27) and (28) are regular expressions so that all limits in Eqs. (29)–(31) can be obtained without involving any singularities.

Substitution of (27) and (28) into (29)–(31) results in a system of $N_p + N_h + 1$ complex algebraic equations, each of which corresponds to an individual inclusion or hole, or the pseudo circular boundary. We write these equations in a condensed form containing three sets of equations as

$$ {}^{\ell}\Omega_{\mathrm{o}}(z) + \sum_{j=1}^{N_p} {}^{\ell}\Omega_j^p(z) + \sum_{j=1}^{N_h} {}^{\ell}\Omega_j^h(z) = 0, \quad (\ell = 1, 2, 3), \tag{32} $$

where $\ell = 1$, 2, and 3 represent the equations for the cases in which evaluation point z is on boundaries Γ_{o}, Γ^p, and Γ^h, respectively. Thus, we have one equation for $\ell = 1$, N_p equations for $\ell = 2$, and N_h equations for $\ell = 3$. Each of the terms ${}^{\ell}\Omega_{\mathrm{o}}(z)$, ${}^{\ell}\Omega_j^p(z)$, and ${}^{\ell}\Omega_j^h(z)$ in (32) is expressed analytically in terms of the basic functions $f_{\mathrm{o}}(z)$, $f_{pj}(z)$, and $f_{hj}(z)$ as well as the unknown coefficients in the Fourier representations on the corresponding boundaries. The detailed expressions can be found in Wang (2004) and are omitted here.

A system of linear algebraic equations needs to be constructed from the set of equations (32) to solve for the unknown coefficients in the series expansions. As mentioned previously, this can be done using an over-specification technique. For the case where all geometric features are circular, however, we have more efficient ways to reduce Eq. (32) to a linear algebraic system. One way is to expand all the functions $f_{\mathrm{o}}^{-m}(z)$, $f_{pj}^m(z)$, and $f_{hj}^m(z)$ and their conjugates into Taylor series with respect to the boundary evaluation point $z \in \Gamma_{\mathrm{o}}$, Γ_k^p, or Γ_k^h around the center z_{o}, z_k^p, or z_k^h of the representative boundary on which z is located such that the left-hand sides of these equations become truncated complex Fourier series. For example, for $\ell = 1$ ($z \in \Gamma_{\mathrm{o}}$) in (32), functions $f_{pj}^m(z)$ and $f_{hj}^m(z)$ and their conjugates are expanded into Taylor series around z_{o} as

$$ f_{*j}^m(z) = \sum_{n=0}^{\infty} (-1)^n \binom{m+n-1}{n} \left(\frac{R_j^*}{R_{\mathrm{o}}}\right)^{m+n} f_{*j}^{-n}(z_{\mathrm{o}}) \cdot f_{\mathrm{o}}^{m+n}(z), \quad (* = p, h), \tag{33} $$

$$ \overline{f_{*j}^m(z)} = \sum_{n=0}^{\infty} (-1)^n \binom{m+n-1}{n} \left(\frac{R_j^*}{R_{\mathrm{o}}}\right)^{m+n} \overline{f_{*j}^{-n}(z_{\mathrm{o}})} \cdot f_{\mathrm{o}}^{-(m+n)}(z), \quad (* = p, h). \tag{34} $$

After doing all such expansions, we group the coefficients of the same power of $f_{\mathrm{o}}(z)$, $f_{pk}(z)$, and $f_{hk}(z)$ and set them equal to zero. By moving all terms involving the boundary loadings [i.e. involving the traction p_j ($j = 1, \ldots, N_h$) and the known coefficients $b_{0\mathrm{o}}$ and $b_{\pm m\mathrm{o}}$ ($m = 1, \ldots, M_{\mathrm{o}}$)] to the right hand side of the equations, we obtain a linear system for the rest of the unknown complex Fourier coefficients: $c_{0\mathrm{o}}$ and $c_{\pm m\mathrm{o}}$ ($m = 1, \ldots, M_{\mathrm{o}}$), b_{0j} and $b_{\pm mj}$ ($m = 1, \ldots, M_{pj}$; $j = 1, \ldots, N_p$), and c_{0j} and $c_{\pm mj}$ ($m = 1, \ldots, M_{hj}$; $j = 1, \ldots, N_h$). This approach is described in detail by Wang et al. (2003b,c).

Another way to obtain the system is to use a Galerkin method as described by Mogilevskaya and Crouch (2001). In this approach, both sides of each equation from the resulting complex system (32) are multiplied by selected weight functions, which are powers of the functions $f_{\mathrm{o}}(t)$, $f_{pk}(z)$, and $f_{hk}(z)$ for $\ell = 1$, 2, and 3, respectively, and then integrated over the representative boundary on which z is located. All of the integrations required to implement the Galerkin procedure can be performed analytically. The linear system obtained in this way is exactly the same as that obtained using Taylor series expansions, but the detailed expressions are omitted here.

It is worth mentioning that the linear system obtained by either approach has a special structure such that each of the complex coefficients for one circular boundary can be expressed explicitly in terms of the coefficients corresponding to other circular boundaries. When partitioning the coefficient matrix of the linear system into N by N blocks ($N = N_p + N_h + 1$), each block on the diagonal of the matrix is itself a diagonal matrix, which represents the self influence corresponding to either the pseudo external boundary

or an individual inclusion or hole. This structure makes it efficient to solve the system using a block Gauss–Seidel iterative method (Mogilevskaya and Crouch, 2001; Wang et al., 2003a). Once the coefficients are found from the linear system, the displacement and stress fields in the domain enclosed by the pseudo circular boundary can be obtained directly by substituting these coefficients into Eqs. (27) and (28). As can be seen from the above discussion, a problem in the circular domain is solved analytically if infinite series are used in the Fourier representations (22)–(25). Apart from round-off, the only errors are due to truncation of the complex Fourier series.

4.4. The solution algorithm

We adopt an iterative algorithm to find the coefficients for the fictitious loading on the pseudo circular boundary such that the boundary conditions on the physical external boundary are satisfied. Once this set of coefficients has been found, the original problem is solved using the solution for its companion problem in the circular embedding domain. In each global iteration, a local block Gauss–Seidel iterative algorithm is first used for computation of the coefficients for each individual inclusion and hole using the coefficients for the fictitious loading; a least squares problem is then solved to update the coefficients for the fictitious loading to satisfy the physical external boundary conditions.

4.4.1. Least squares formulation

The least squares problem is formulated as follows. We choose M_c uniformly distributed control points on the physical external boundary Γ_e, where M_c^t points are on the traction-prescribed part $\Gamma_e^{(t)}$ and M_c^u points are on the displacement-prescribed part $\Gamma_e^{(u)}$ $(M_c^t + M_c^u = M_c)$. The tractions at the control points on $\Gamma_e^{(t)}$ can be written in a real vector as

$$\mathbf{t} = \{t_x(z_1), t_y(z_1), \ldots, t_x(z_{M_c^t}), t_y(z_{M_c^t})\}^{\mathrm{T}}. \tag{35}$$

In expression (28), the stress components $S_m^{(o)}(z)$ and $S_d^{(o)}(z)$ contributed directly from the pseudo circular boundary Γ_o can be further decomposed as

$$S_m^{(o)}(z) = S_{mb}^{(o)}(z) + S_{mc}^{(o)}(z), \quad S_d^{(o)}(z) = S_{db}^{(o)}(z) + S_{dc}^{(o)}(z), \tag{36}$$

where $S_{mb}^{(o)}(z)$ and $S_{db}^{(o)}(z)$ are expressed in terms of the coefficients in the Fourier expansion for the fictitious tractions, and $S_{mc}^{(o)}(z)$ and $S_{dc}^{(o)}(z)$ in terms of the coefficients in the Fourier expansion for the fictitious displacements. As a result, the traction vector (35) can be written as a summation of three vectors $\mathbf{t}_b^{(o)}$, $\mathbf{t}_c^{(o)}$, and $\mathbf{t}^{(i)}$, where $\mathbf{t}_c^{(o)}$ and $\mathbf{t}^{(i)}$ can be calculated from the corresponding stress components in (36), (28), and the relation (14) using the solution for the coefficients in the series expansion. Each component of the vector $\mathbf{t}_b^{(o)}$ can be expressed in terms of the coefficients (b_{0o} and $b_{\pm mo}$) for the fictitious tractions using the relation

$$t_b^{(o)}(z_k) = n(z_k) S_{mb}^{(o)}(z_k) - \overline{n(z_k)}\,\overline{S_{db}^{(o)}(z_k)}, \quad (z_k \in \Gamma_e^{(t)};\ k = 1, \ldots, M_c^t). \tag{37}$$

After separating the real and imaginary parts, we can write (37) in a matrix form as

$$\mathbf{t}_b^{(o)} = \mathbf{A}_t \mathbf{x}, \tag{38}$$

where $\mathbf{x}$ is the vector composed of the coefficients for the fictitious tractions,

$$\mathbf{x} = \{\mathrm{Re}\, b_{-M_o o}, \mathrm{Im}\, b_{-M_o o}, \ldots, \mathrm{Re}\, b_{-2o}, \mathrm{Im}\, b_{-2o}, b_{0o}, \mathrm{Re}\, b_{1o}, \mathrm{Im}\, b_{1o}, \ldots, \mathrm{Re}\, b_{M_o o}, \mathrm{Im}\, b_{M_o o}\}^{\mathrm{T}} \tag{39}$$

and the real coefficient matrix $\mathbf{A}_t$ is of size $(2M_c^t)$ by $(4M_o - 1)$. By satisfying the prescribed traction boundary conditions at all control points on $\Gamma_e^{(t)}$, we have

$$\mathbf{A}_t \mathbf{x} = \mathbf{g}_t, \quad \text{and} \quad \mathbf{g}_t = \mathbf{t}^{\mathrm{pr}} - \mathbf{t}_c^{(o)} - \mathbf{t}^{(i)}, \tag{40}$$

where $\mathbf{t}^{\mathrm{pr}}$ is a vector obtained from (17) for prescribed tractions at the control points on $\Gamma_e^{(t)}$.

Similarly, the real displacement vector for the control points on $\Gamma_{\mathrm{e}}^{(u)}$,

$$\mathbf{u} = \{u_x(z_1), u_y(z_1), \ldots, u_x(z_{M_{\mathrm{c}}^u}), u_y(z_{M_{\mathrm{c}}^u})\}^{\mathrm{T}}$$

can be written as a summation of three vectors $\mathbf{u}_{\mathbf{b}}^{(\mathbf{o})}$, $\mathbf{u}_{\mathbf{c}}^{(\mathbf{o})}$, and $\mathbf{u}^{(\mathbf{i})}$, where $\mathbf{u}_{\mathbf{c}}^{(\mathbf{0})}$ and $\mathbf{u}^{(\mathbf{i})}$ can be calculated directly from the corresponding terms in (27), and $\mathbf{u}_{\mathbf{b}}^{(\mathbf{o})}$ can be expressed in the following form

$$\mathbf{u}_{\mathbf{b}}^{(\mathbf{o})} = \mathbf{A}_{\mathbf{u}}\mathbf{x}, \tag{41}$$

where $\mathbf{x}$ is the same as (39) and the coefficient matrix $\mathbf{A}_{\mathbf{u}}$ is of size $(2M_{\mathrm{c}}^u)$ by $(4M_{\mathrm{o}} - 1)$. By satisfying the prescribed displacement boundary conditions at all control points on $\Gamma_{\mathrm{e}}^{(u)}$, we have

$$\mathbf{A}_{\mathbf{u}}\mathbf{x} = \mathbf{g}_{\mathbf{u}}, \quad \text{and} \quad \mathbf{g}_{\mathbf{u}} = \mathbf{u}^{\mathrm{pr}} - \mathbf{u}_{\mathbf{c}}^{(\mathbf{0})} - \mathbf{u}^{(\mathbf{i})}, \tag{42}$$

where the vector $\mathbf{u}^{\mathrm{pr}}$ is obtained from (18) for prescribed displacements at the control points on $\Gamma_{\mathrm{e}}^{(u)}$.

Combining (40) and (42), we have the following overspecified system

$$\mathbf{A}\mathbf{x} = \mathbf{g}, \quad \text{where } \mathbf{A} = \begin{pmatrix} \mathbf{A}_{\mathbf{t}} \\ \mathbf{A}_{\mathbf{u}} \end{pmatrix} \quad \text{and} \quad \mathbf{g} = \begin{pmatrix} \mathbf{g}_{\mathbf{t}} \\ \mathbf{g}_{\mathbf{u}} \end{pmatrix}, \tag{43}$$

where $\mathbf{A} \in \mathbb{R}^{n_p \times n_q}$ ($n_p = 2M_{\mathrm{c}}$ and $n_q = 4M_{\mathrm{o}} - 1$), and $K_{\mathrm{o}} = n_p/n_q$ is the overspecification factor. Applying the discrete least squares condition expressed in (20), we can solve this system via a reduced QR decomposition (Golub and Van Loan, 1996),

$$\mathbf{A} = \mathbf{Q}\mathbf{R} \ (\mathbf{Q} \in \mathbb{R}^{n_p \times n_q}, \mathbf{R} \in \mathbb{R}^{n_q \times n_q}). \tag{44}$$

The column vectors of $\mathbf{Q}$ are orthonormal to each other and R is an upper triangular matrix. The solution to (43) is then obtained by solving the following linear system using back substitution

$$\mathbf{R}\mathbf{x} = \mathbf{Q}^{\mathrm{T}}\mathbf{g}. \tag{45}$$

4.4.2. The iterative algorithm

Prior to the iteration process, we need to choose a value for the number of terms M_{pj} ($j = 1, \ldots, N_p$), M_{hj} ($j = 1, \ldots, N_h$), and M_{o} in the Fourier series for each circular boundary. Further discussion on the choice of these numbers is presented in Section 4.4.3. We also need to initialize the values of all the Fourier coefficients for each inclusion, hole, and the pseudo boundary; usually, these are set to zero. The solution procedure is summarized as follows:

1. Construct the matrix $\mathbf{A}$ according to (43) and compute its reduced QR decomposition as (44);
2. Give an initial distribution of the fictitious traction $\sigma_{\mathrm{o}}(z)$ on the pseudo circular boundary Γ_{o} with known coefficients $b_{0\mathrm{o}}$ and $b_{\pm m\mathrm{o}}$ ($m = 1, \ldots, M_{\mathrm{o}}$);
3. Solve for all the other coefficients $c_{\pm m\mathrm{o}}$ ($m = 1, \ldots, M_{\mathrm{o}}$), b_{0j} and $b_{\pm mj}$ ($m = 1, \ldots, M_{pj}$; $j = 1, \ldots, N_p$), and $c_{\pm mj}$ ($m = 1, \ldots, M_{hj}$; $j = 1, \ldots, N_h$) from the linear system obtained in Section 4.3 using a single Gauss–Seidel iteration;
4. Using the immediate solution obtained in step 3, calculate the vector $\mathbf{g}$ in (43) and the product $\mathbf{Q}^{\mathrm{T}}\mathbf{g}$;
5. Solve the linear system expressed in (45) for a new version of the coefficients $b_{0\mathrm{o}}$ and $b_{\pm m\mathrm{o}}$;
6. Repeat steps 3–5 until the largest relative change in the coefficients between two successive iterates is less than a small number ε (say $\varepsilon = 10^{-8}$).

It is worth mentioning that from our experience it is not necessary to repeat step 3 in the above algorithm until the local Gauss–Seidel iteration converges. In order to achieve global convergence in a small number of iterations with relatively little computational effort, we incorporate the local iterations into the global iteration and do only one Gauss–Seidel iteration in step 3. In this way the coefficients for the fictitious load-

ing are updated once updated versions of all other coefficients are available. We find from extensive numerical experiments that this combination of the two iteration processes gives the best performance of the algorithm.

4.4.3. Determination of the number of terms in the Fourier expansions

The procedure we have adopted to determine the number of terms in the Fourier expansions is similar to that described by Crouch and Mogilevskaya (2003). We define two reference quantities t_{ref} and u_{ref} for the tractions and displacements as

$$t_{\text{ref}} = \max(|\, t^{\text{pr}} \,|, |\, u^{\text{pr}} \,| E_{\text{m}}/L_{\text{e}}) \quad \text{and} \quad u_{\text{ref}} = \max(|\, u^{\text{pr}} \,|, |\, t^{\text{pr}} \,| L_{\text{e}}/E_{\text{m}}), \tag{46}$$

where t^{pr} and u^{pr} are the prescribed traction and displacements on the external boundary; L_{e} is the perimeter of Γ_{e}; E_{m} is the Young's modulus of the material matrix. Suppose that the Fourier coefficients have been calculated for fixed values of M_{pj}, M_{hj}, and M_{o} according to the numerical procedure outlined in Section 4.4.2. We estimate the errors at each boundary as follows to determine if the current number of terms is sufficient:

1. For hole j ($j = 1, \ldots, N_h$), we calculate the tractions from (14) and (28) at a set of uniformly distributed points on the boundary and compute $\Delta t_{\max}$, the magnitude of the largest difference between these values and the prescribed tractions at these points. If $\Delta t_{\max}/t_{\text{ref}} \leqslant \delta_{\text{i}}$ (δ_{i} is a specified small number, say 10^{-6}), we keep M_{hj} unchanged; otherwise, we increase the value of M_{hj} by ΔM_{hj};
2. Similarly, for inclusion j ($j = 1, \ldots, N_p$), we calculate the boundary tractions from (14) and (28) at selected points and compute $\Delta t_{\max}$ between these tractions and those calculated from (24). By checking if the condition $\Delta t_{\max}/t_{\text{ref}} \leqslant \delta_{\text{i}}$ is satisfied, we determine whether to increase M_{pj} by ΔM_{pj};
3. For the finite external boundary Γ_{e}, we calculate the boundary tractions and displacements at the control points over $\Gamma_{\text{e}}^{(t)}$ and $\Gamma_{\text{e}}^{(u)}$, respectively. The errors ϵ_t and ϵ_u are calculated as

$$\epsilon_t = \sqrt{\sum_{k=1}^{M_{\text{c}}^t} [t(z_k) - t^{\text{pr}}(z_k)]^2 \big|_{z_k \in \Gamma_{\text{e}}^{(t)}}} \quad \text{and} \quad \epsilon_u = \sqrt{\sum_{k=1}^{M_{\text{c}}^u} [u(z_k) - u^{\text{pr}}(z_k)]^2 \big|_{z_k \in \Gamma_{\text{e}}^{(u)}}}. \tag{47}$$

   For a small specified number δ_{o}, we check if the condition $\max(\epsilon_t/t_{\text{ref}}, \epsilon_u/u_{\text{ref}}) \leqslant \delta_{\text{o}}$ is satisfied. If not, M_{o} is increased by ΔM_{o}.

In the above error checking procedure, the ΔM's (ΔM_{hj}, ΔM_{pj}, and ΔM_{o}) are usually chosen between 1 and 10 depending upon the magnitude of relative errors on the corresponding boundaries. After examining all the boundaries, if any value of M_{pj}, M_{hj}, and M_{o} has been changed, the iterative process described in Section 4.4.2 needs to be repeated, and the current values of the Fourier coefficients are used as initial approximations. In order to avoid repeating the iterative process, we could choose sufficiently large values of M_{pj}, M_{hj}, and M_{o} at the beginning so that all the boundary conditions are satisfied to within a specified degree of accuracy after the first stage of iteration. This approach may use more storage for the extra terms than is actually required, but the procedure is easier to implement and in many cases turns out to be more computationally efficient. Some experience is required, however, to select values of the M's that are not excessively large.

4.5. A modification of the embedding method

In the above formulation of the embedding method, we have two sets of Fourier series defined on the boundary of the embedding circular domain, one for fictitious tractions and the other for fictitious

displacements. We observe from the expressions (A.1) and (A.4) that the potentials arising from the boundary conditions of the fictitious embedding domain can be expressed in terms of one series expansion with the coefficients defined as a combination of the coefficients in the Fourier expansions for the fictitious tractions and displacements. As a result, the solution algorithm described above can be slightly modified to avoid separate calculation of the fictitious tractions and displacements on the pseudo circular boundary. Instead, the combined influence of these quantities can be calculated.

In this new formulation, we combine the two sets of coefficients in (22) and (23) for the fictitious tractions and displacements into one set of coefficients q_0 and $q_{\pm m}$ $(m = 1, \ldots, M_o)$,

$$\begin{aligned} q_{-m} &= m\frac{c_{-mo}}{R_o} + \frac{\kappa_m}{2\mu_m} b_{-(m+1)o}, \quad (m = 1, \ldots, M_o), \\ q_m &= (m+1)\frac{c_{(m+1)o}}{R_o} + \frac{1}{2\mu_m} b_{mo}, \quad (m = 0, \ldots, M_o). \end{aligned} \tag{48}$$

The potentials $\varphi^{(o)}(z)$ and $\psi^{(o)}(z)$ in (12) can now be expressed in terms of the new coefficients q_0 and $q_{\pm m}$. The expressions are given in Appendix B as (B.1) and (B.2), reduced from (A.1) and (A.4). As a result, the displacement function $u^{(o)}(z)$ in (27) and the stress components $S_m^{(o)}(z)$ and $S_d^{(o)}(z)$ in (28) can also be expressed directly in terms of the new set of coefficients defined in (48). According to this new formulation, the solution algorithm is similar to that described in the Section 4.4.2, except that the matrices $\mathbf{A_t}$ and $\mathbf{A_u}$ are formulated based on the new expressions for $S_m^{(o)}(z)$, $S_d^{(o)}(z)$ and $u^{(o)}(z)$ and that the vectors $\mathbf{g_t}$ and $\mathbf{g_u}$ are expressed as follows instead of as in (40) and (42),

$$\mathbf{g_t} = \mathbf{t}^{pr} - \mathbf{t}^{(i)} \quad \text{and} \quad \mathbf{g_u} = \mathbf{u}^{pr} - \mathbf{u}^{(i)}. \tag{49}$$

4.6. Location and radius of the circular embedding domain

Theoretically, the location and the radius of the embedding domain can be arbitrary as long as the physical solution domain is entirely embedded within it. The center z_o of the embedding domain usually coincides with the center of the physical domain. We may, however, encounter computational difficulty if R_o is too large because in this case the values of the elementary functions $f_o^{\pm m}(z)$ might be too large or too small for some large values of m, which may increase the condition number of the system and thus the associated numerical errors. This problem, however, can be treated by a simple scaling,

$$f_o^{\pm m}(z) = \left(\frac{R_s}{z - z_o}\right)^{\pm m} \left(\frac{R_o}{R_s}\right)^{\pm m}, \tag{50}$$

where R_s is chosen such that the pseudo circular boundary is as close to the physical external boundary as possible; $(R_o/R_s)^{\pm m}$ can be incorporated into the coefficients in the series expansions and do not need to be evaluated directly. As a result, we only need to choose a value for R_s in our computations. According to our experience, for a rectangular physical solution domain with the half-diagonal length equal to R_d, the optimum value for R_o/R_d is between 1.0 and 1.5. With the scaling employed, however, the ratio R_s/R_d is usually chosen within a range of 0.7–1.5.

5. Numerical experiments

For a particular problem, the overspecification factor K_o, the ratio of R_s/R_d, and the parameters for error control ε, δ_i, and δ_o are predetermined. In the following numerical experiments, if not otherwise specified, K_o was taken as 3; R_s/R_d was chosen to be 0.8; the iteration tolerance limit ε was taken as 10^{-8}; the accuracy levels for the internal boundaries and the external boundary, δ_i and δ_o, were taken as 10^{-6} and

10^{-4}, respectively. As described in Section 4.4.3, the numbers of terms in the Fourier expansions M_{pj}, M_{hj}, and M_o were chosen in such a way that the corresponding boundary conditions are satisfied within the specified accuracy levels.

5.1. Test examples

5.1.1. One inclusion in a rectangular plate

As the first example, we consider a circular inclusion or hole of radius R centered in a rectangular plate with height $2h$ and width $2w$. A uniform normal traction $t_y^{\mathrm{pr}} = 1$ is prescribed on two opposite sides of the plate (Fig. 3). The elastic properties of the inclusion and matrix are μ_i, ν_i and μ_{m}, ν_{m}, respectively. For the limiting case when $\mu_i = 0$, the inclusion becomes a hole. A state of plane strain is assumed. Our interest here is the stress concentration factor K_t, which is defined as the maximum absolute value of the normalized circumferential stress $\widehat{\sigma}_{\theta\theta} = \sigma_{\theta\theta}/t_y^{\mathrm{pr}}$:

$$K_t = \begin{cases} \max(\max\limits_{z\in\Gamma^p} \mid \widehat{\sigma}^{+}_{\theta\theta}(z) \mid, \quad \max\limits_{z\in\Gamma^p} \mid \widehat{\sigma}^{-}_{\theta\theta}(z) \mid) & \text{for inclusion,} \\ \max\limits_{z\in\Gamma^h} \mid \widehat{\sigma}_{\theta\theta}(z) \mid & \text{for hole.} \end{cases} \tag{51}$$

where the $+(-)$ indicates that point z approaches the boundary from the inside (outside) of the inclusion.

For the right setup in Fig. 3, we consider the following four cases: (i) $h/w = 1$, $R/w = 0.5$; (ii) $h/w = 1$, $R/w = 0.1$; (iii) $h/w = 2$, $R/w = 0.5$; (iv) $h/w = 2$, $R/w = 0.1$. The value of K_t for case (i) was computed by Isida and Sato (1984) using a method based on series expansions, and by Helsing and Jonsson (2002) using a collocation boundary element method based on singular integral equations. Isida and Sato reported a value $K_t = 6.3887$. Helsing and Jonsson computed the values of K_t using different numbers of discretization points and gave the converged result of $K_t = 6.3886960194568$, which was reached at about 2000 discretization points. We choose the number of terms in the Fourier expansion for the hole equal to 20. The convergence of our numerical results of K_t for cases (i) and (ii) with the increase of the number of terms M_o in the Fourier expansion for the fictitious loading is shown in Fig. 4. The relative errors are computed using with a reference value taken as the above value of K_t by Helsing and Jonsson (2002). As can be seen from Fig. 4, our results converged rapidly with the increase of M_o and, with a relatively small number of terms in the series expansion, our method gives numerical results with desirable accuracy. The value of K_t for case (i) is also computed for different values of R_s/R_d between 0.7 and 2.0 other than 0.8 with M_o equal to 30. The computed value for K_t was 6.388694 in each instance. We computed the other three cases with R_s/R_d taken

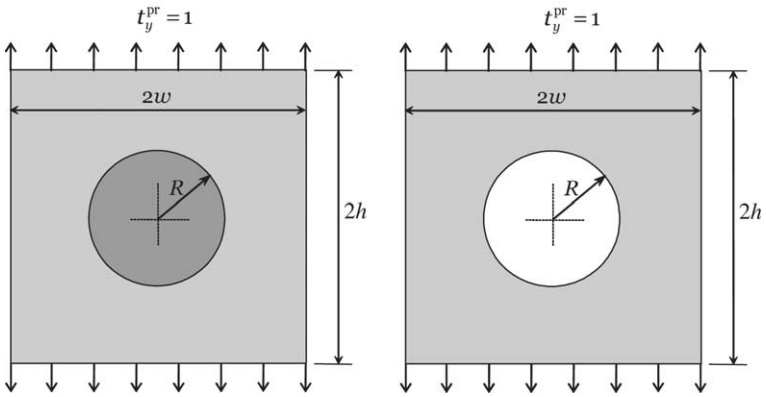

Fig. 3. One inclusion (left) or hole (right) in a rectangular plate subjected to uniaxial tension.

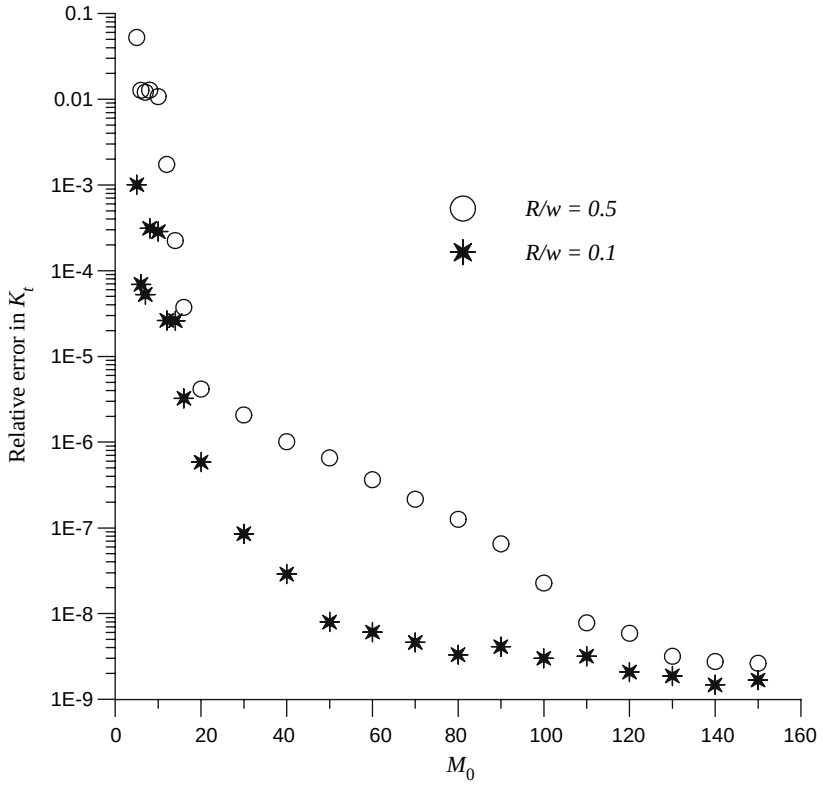

Fig. 4. Convergence of the stress concentration factor K_t for a circular hole of radius R centered at a square plate of width w. The relative errors are computed with a reference value taken as $K_t = 6.3886960194568$.

as 0.8 and M_o equal to 40. It is found that the height-width ratio h/w has a significant effect on the stress concentration factor for relatively large values of R/w. With a decrease of R/w, however, the results become less sensitive to the ratio of h/w. In the case of $R/w = 0.1$, the results are very close to those for a hole in an infinite plate. Most of our computations converged in 20–25 iterations and took only a few seconds on a 1.5 GHz PC.

We also computed the circumferential stress for an inclusion with elastic properties μ_i and ν_i different from those of the matrix, μ_m and ν_m. A setup with $h/w = 1.0$ and $R/w = 0.5$ is considered. We solve the problem for different values of the inclusion-matrix shear modulus ratio $\gamma = \mu_i/\mu_m$ with $\nu_i = \nu_m = 0.3$. Fig. 5 shows the variation of the stress concentration factor K_t with γ, calculated from (51). When the inclusion is softer than the matrix, the stress concentration factor decreases rapidly with the increase of γ; it increases very slowly with the increase of γ when the inclusion is stiffer than the matrix.

5.1.2. Multiple holes in a rectangular plate

In this section, we consider several examples that appear many times in the literature but with no uniform results obtained. Our computations disprove some published results and provide the corresponding new benchmark results. The first example is about four small equal-sized holes with radius R placed in a rhombic pattern in a square plate with side length equal to $2w$. Uniform normal traction is prescribed on two opposite sides of the plate (see Fig. 6). The centers of the holes are located at points $(d, 0)$, $(0, d)$, $(-d, 0)$, and $(0, -d)$. Using the embedding method, we compute the maximum stress concentration in the

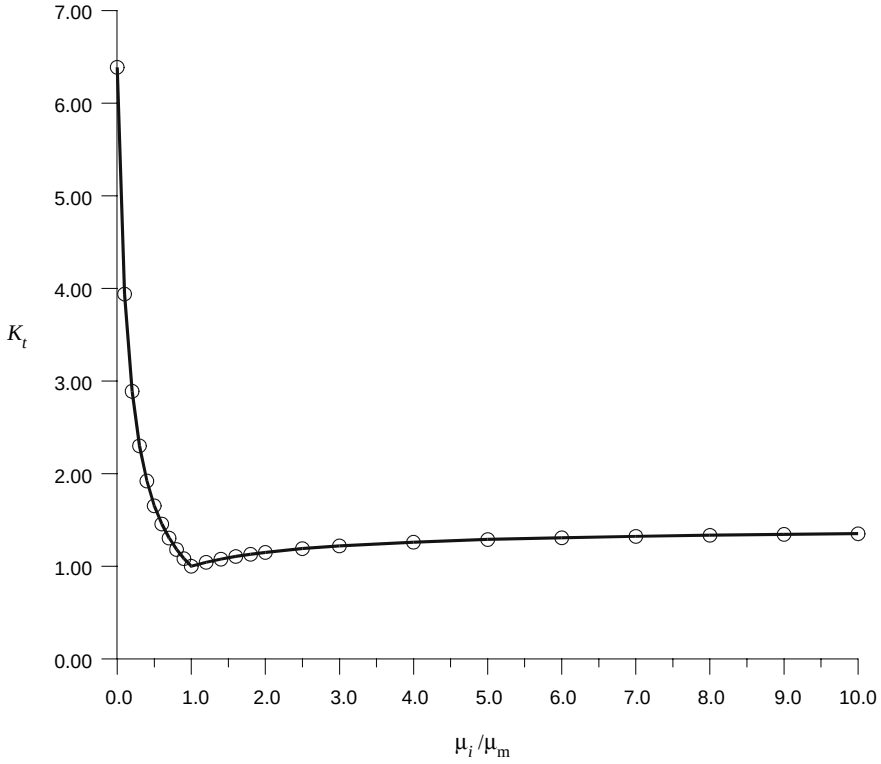

Fig. 5. Variation of K_t on the boundary of the inclusion with the inclusion-matrix shear modulus ratio.

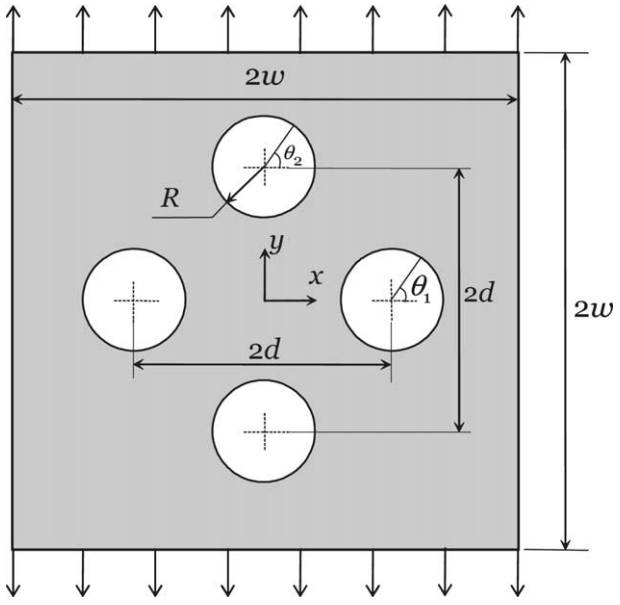

Fig. 6. Four holes in a square plate subjected to uniaxial tension.

plate for a setup with $R/w = 0.15$ and d varying from $2R$ to $5R$, in which some of Helsing and Jonsson's (2002) results are considerably different from those by Woo and Chan (1992). To achieve the predetermined accuracy levels ($\delta_i = 10^{-6}$ and $\delta_o = 10^{-4}$), we use 20 terms of Fourier series for each hole and take $M_o = 40$ for all cases other than $d/R = 5$. For the latter case, the number of Fourier terms for the holes is increased to 30 and M_o to 80. Helsing and Jonsson's (2002), Woo and Chan's (1992), and our results are listed in Table 1. Good agreement can be seen between our results and those obtained by Helsing and Jonsson (2002). The locations where the maximum stress concentration factor occurs given in Table 1 refer to the holes centered at $(d, 0)$ and $(0, d)$.

We now consider a more complex hole system involving five symmetrically aligned holes in a rectangular plate with $h/w = 3.125$, as depicted in Fig. 7. The plate is subjected to a uniform normal traction in the vertical direction. The two holes at the top and bottom of the plate have radii $R_1 = R_5 = 0.25w$, and the one in the middle has radius $R_3 = w/16$. The radii of the two other holes, R_2 and R_4, vary between $w/16$

Table 1
Results for the stress concentration factor K_t in a square plate containing four holes

d/R	Woo and Chan (1992)	Helsing and Jonsson (2002)	Embedding method
2.0	4.833	4.83267	4.83267 at $\theta_1 = 0°$
2.5	4.332	4.33144	4.33144 at $\theta_1 = 180°$
3.0	4.051	4.05049	4.05049 at $\theta_1 = 180°$
3.5	3.814	3.81430	3.81430 at $\theta_1 = 180°$
4.0	3.768	3.76936	3.76936 at $\theta_2 = 0.2°$ and 179.8°
4.5	3.860	3.94144	3.94144 at $\theta_1 = 0°$
5.0	3.905	4.7639	4.7637 at $\theta_1 = 0°$

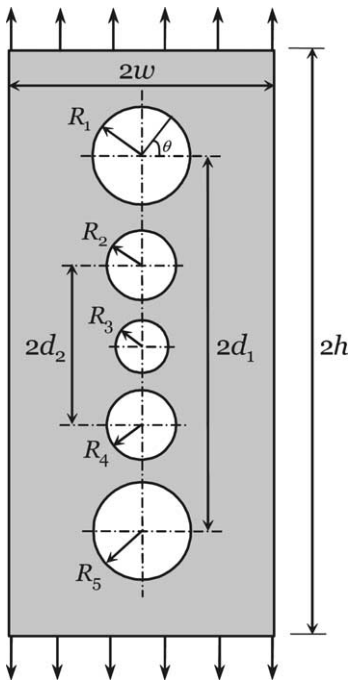

Fig. 7. Symmetrically placed holes in a rectangular plate subjected to uniaxial tension.

and $11w/48$. The separation distances are $d_1 = 5w/6$ and $d_2 = w/3$. This problem was solved by Chen et al. (2000) using a boundary element alternating method, by Meguid (1986) using finite element analysis, and by Helsing and Jonsson (2002) using a collocation boundary element method. The results for the stress concentration factor at the top hole are compared with those obtained using the embedding method in Table 2. In our analysis, thirty terms of Fourier series were used for all the holes and M_o was taken as 80. It can be seen from Table 2 that our results agree well with the converged results obtained in Helsing and Jonsson (2002).

As another example, we solve a problem of two closely spaced holes in a square plate involving both traction and displacement boundary conditions. As shown in Fig. 8, one of the two vertical sides of the plate is subjected to uniform normal displacement of 1 mm; the two horizontal sides are traction free. A state of plane stress is assumed. The side length of the square plate is $a = 100$ mm, and the two holes are of the same radius $R = 5$ mm. The holes are aligned along the horizontal symmetry line and are of the same distance from the center of the plate, with the minimum separation between them equal to $d = 0.5$ mm. The material properties of the matrix are $E = 10$ MPa, $v = 0.3$. Kong et al. (2002) analyzed this problem using their two-dimensional boundary element software THBEM2. They compared their results for the Von-Mises stress on the boundaries of the holes with the finite element results obtained using MSC/Marc software and observed a big difference. Skeptical about their results, we solved the problem using both the embedding method and the finite element software ANSYS. In the embedding approach, we chose $M_o = 80$ for the pseudo circular boundary and 40 terms of Fourier series for each hole; in the finite element analysis, we used 13,844 eight-node quadratic elements of the type PLANE82. The results

Table 2
Results for the stress concentration factor K_t for the top hole in Fig. 7

$R_2 = R_4$	Meguid (1986)	Chen et al. (2000)	Helsing and Jonsson (2002)	Embedding method
$w/16$	3.244	3.115	3.119174	3.119174 at $\theta = 1.5°$ and 178.5°
$w/12$	3.204	3.102	3.106916	3.106915 at $\theta = 1.7°$ and 178.3°
$w/6$	3.049	2.980	2.996977	2.996976 at $\theta = 3.2°$ and 176.8°
$11w/48$	2.981	2.792	2.830921	2.830919 at $\theta = 4.9°$ and 175.1°

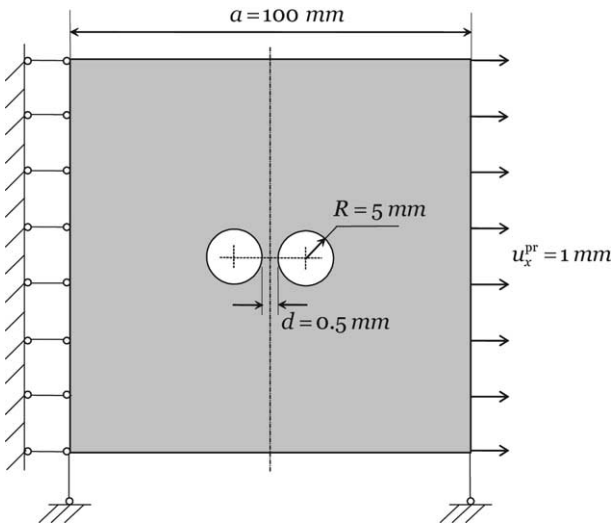

Fig. 8. A square plate with two closely spaced circular holes under given uniform displacement on one side.

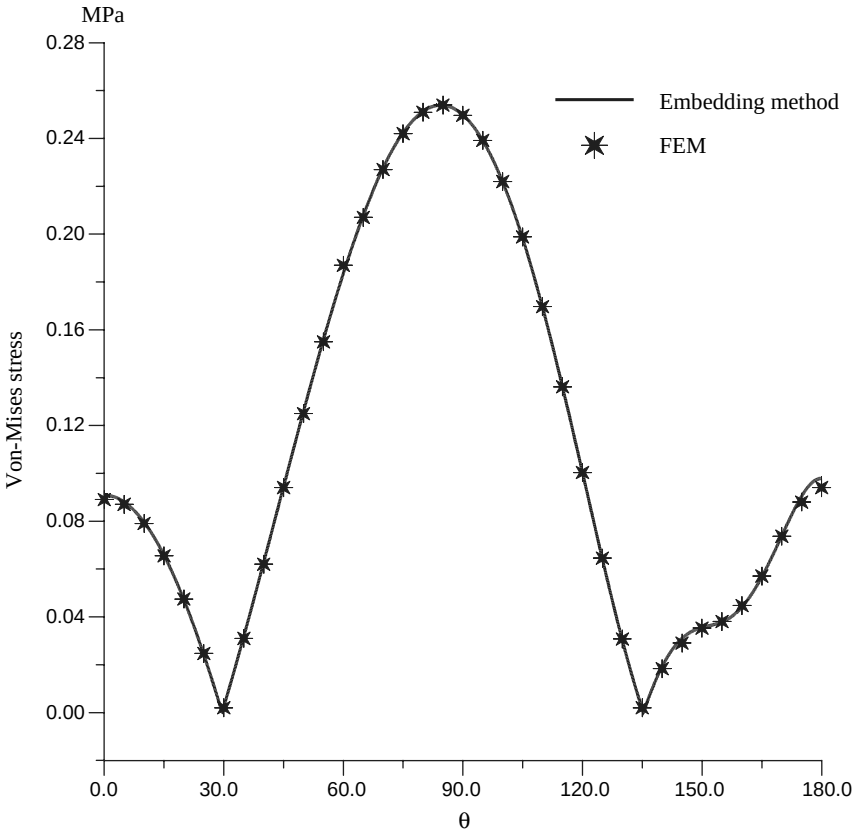

Fig. 9. The Von-Mises stress on the boundary of the right hole in Fig. 8.

we obtained from two independent approaches are in good agreement, as plotted in Fig. 9. The only difference we observed occurs in the vicinity of the close-to-touching points of the two holes, where it is very difficult for the finite element method to get accurate results.

5.2. Large scale computations

In the last example, we model a fiber-reinforced composite with fibers distributed in a square pattern. The elastic properties of the fiber and matrix material are μ_i, ν_i and μ_{m}, ν_{m}, respectively. Plane strain conditions are assumed for the corresponding two-dimensional model shown in Fig. 10. In the left setup of Fig. 10, one inclusion of radius R is located in the center of a square plate of width $2w$ and $R/w = 0.5$. Taking this configuration as a basic cell and reproducing it in a square grid, we obtain a relatively large setup, in which a square of width $2w$ contains $N_p = n^2$ equal-sized inclusions of the radii $0.5w/n$. Two different types of boundary conditions are considered: (i) edges AB and CD are subjected to uniform tension t_y^{pr}, BC and AD are traction free; (ii) edge AB is fixed in the vertical direction and CD is subjected to uniform vertical displacement, BC and AD remain straight after deformation.

We first compute the maximum stress concentration factor K_t inside the plate under loading condition (i) for different values of n. We take $\nu_{\mathrm{m}} = \nu_i = 0.3$ and let the rigidity ratio between the fibers and the matrix $\gamma = \mu_i/\mu_{\mathrm{m}}$ vary from 0 to 10,000, where $\gamma = 0$ represents the limiting case corresponding to empty fibers (holes) and $\gamma = 10{,}000$ can be used to approximate the case of rigid fibers. Our results for the maximum

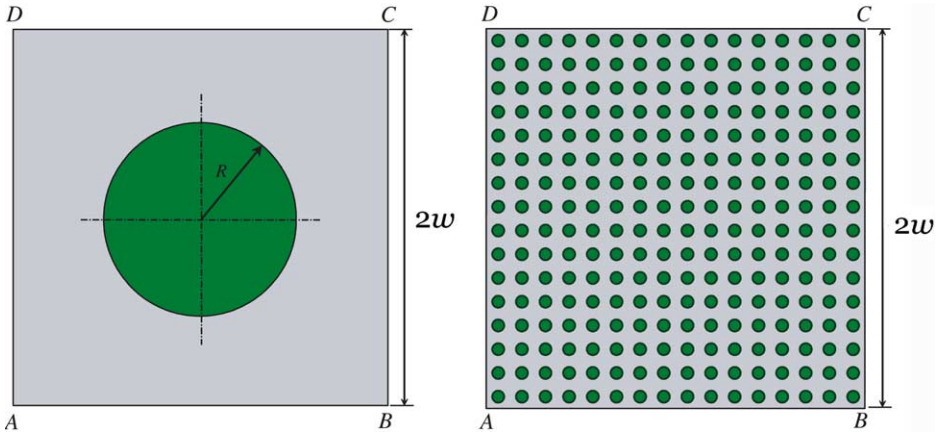

Fig. 10. A square plate containing n^2 inclusions ($n = 1$ for the left setup and $n = 16$ for the right one).

Table 3
Results for the maximum stress concentration factor K_t for different values of γ

n	N_p	$\gamma = \mu_i/\mu_m$									
		0	0.1	0.2	0.5	2	5	10	100	1000	10,000
1	1	6.389	3.940	2.890	1.654	1.150	1.289	1.352	1.422	1.430	1.431
2	4	4.538	3.300	2.598	1.604	1.166	1.320	1.390	1.467	1.475	1.476
4	16	4.580	3.308	2.600	1.604	1.166	1.320	1.390	1.467	1.476	1.477
8	64	4.580	3.308	2.600	1.604	1.166	1.320	1.390	1.467	1.476	1.476
16	256	4.579	3.308	2.600	1.604	1.166	1.320	1.390	1.467	1.476	1.476
32	1024	4.579	3.308	2.600	1.604	1.166	1.320	1.390	1.467	1.476	1.476

Table 4
Results of the maximum stress concentration factor K_t for $\gamma = 0$

n	N_h	Embedding method	ANSYS
1	1	6.388696 at $\theta = 0°$ and 180°	6.389
2	4	4.53846 at $\theta = 186.1°$	4.538
4	16	4.57954 at $\theta = 185.9°$	4.580
8	64	4.57963 at $\theta = 185.9°$	4.580
16	256	4.5793 at $\theta = 185.9°$	4.579

values of the stress concentration factor K_t in the plate for different values of γ and different numbers of inclusions are given in Table 3. It is observed that the results tend to limiting values with increased γ and that the results converge with increase of the number of inclusions. For the limiting case of $\gamma = 0$, more detailed results for the maximum values of K_t and the corresponding locations on the hole at the left lower corner are given in Table 4. As an independent check on this case, a finite element analysis using ANSYS was performed. According to the symmetry of the problem, we model a quarter of the plate using the eight-node quadratic elements of type PLANE82. A multi-level local refinement of the mesh near the hole at the corner is adopted. More than 20,000 elements were used for each case to obtain the converged results listed

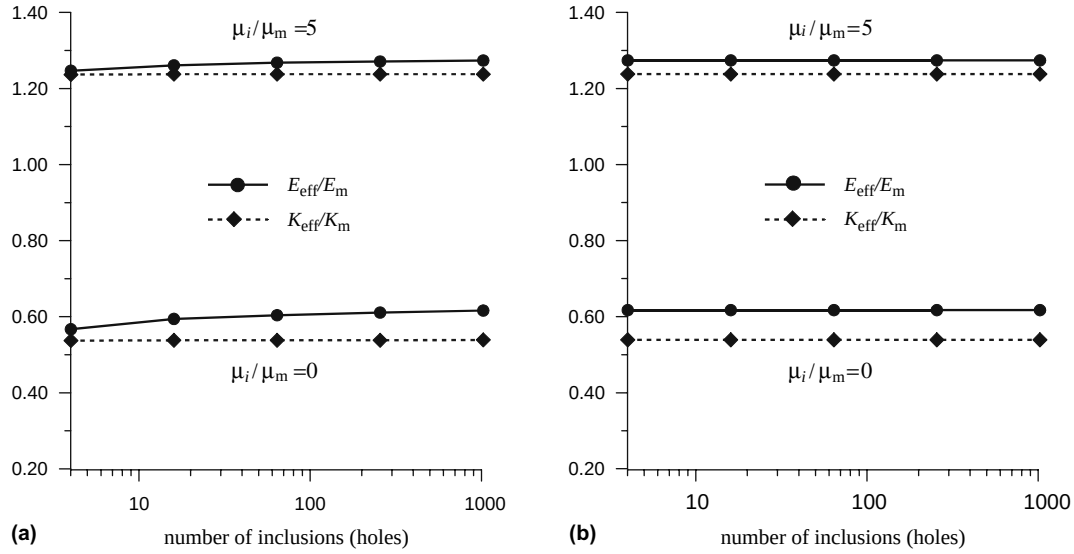

Fig. 11. Convergence of the results for the effective properties for (a) traction and (b) displacement boundary conditions.

in Table 4. For example, the results for $n = 8$ were obtained using 35,488 elements and for $n = 16$ using 44,336 elements. The results obtained using the embedding method agree with the ANSYS results.

We also compute the effective properties of the fiber-reinforced composite using the above computational model. The effective elastic constants are calculated from the average stresses and strains inside material, which can be obtained directly from the boundary tractions and displacements (see, for example, Wang, 2004). Taking $v_i = v_m = 0.3$, we consider $\gamma = 0$ and $\gamma = 5$ for a fiber volume ratio equal to $\pi/16$. The normalized two-dimensional plane strain bulk modulus K_{eff}/K_m and Young's modulus E_{eff}/E_m are computed for two different types of boundary conditions stated above: (i) a traction boundary condition and (ii) a straight-line displacement boundary condition. The corresponding results are plotted in Fig. 11 for different numbers of fibers. The largest setup contains 1024 fibers or holes. It is observed that the computed results for the effective elastic constants converge rapidly with the increase of the number of inclusions or holes for traction boundary conditions and that the results are essentially constant for straight-line displacement boundary conditions. Based on this observation, we conclude that the displacement boundary conditions are better suited for computation of the effective properties.

6. Concluding remarks

In this paper an embedding method is presented to extend our numerical technique for solving problems of multiple circular holes and elastic inclusions in a finite circular domain (Wang et al., 2003c) to finite domains with rectangular external boundaries, with application to fiber-reinforced composite and perforated materials. In a sense, the method can be viewed as a meshless method, because it requires no discretization of the boundaries. By embedding the solution domain into a fictitious circular domain, all integrals involved in this method are evaluated analytically. The method is capable of providing results of high accuracy for relatively low computational cost. With this method, problems of large size that are very difficult to handle with conventional methods can easily and quickly be solved on a personal computer.

Refinements and extensions of this method are planned in several respects. The first natural extension is the incorporation of cracks based on the work reported in Wang et al. (2001, 2003b). Another extension of the method is to use a fictitious elliptical domain instead of a circle. We expect that an elliptical shape will be better suited for problems in an elongated domain, e.g. a rectangular domain with large height–width ratio. We also plan to extend the methodology to three dimensions for modeling particle-reinforced composite materials.

Appendix A. Expressions for potentials

The complex potentials $\varphi(z)$ and $\varphi(z)$ are written by summation of the influence from the pseudo circular boundary and the individual holes and inclusions as in (11), with each term in (12) given below:

$$\varphi^{(\mathrm{o})}(z) = \eta \sum_{m=0}^{M_\mathrm{o}} \left[\frac{c_{m\mathrm{o}}}{f_\mathrm{o}^m(z)} + \frac{R_\mathrm{o}}{2\mu_\mathrm{m}} \frac{b_{m\mathrm{o}}}{(m+1) f_\mathrm{o}^{m+1}(z)} \right], \tag{A.1}$$

$$\varphi_j^p(z) = \eta a_{1j} R_j^p \times \begin{cases} \sum_{m=0}^{M_{pj}} \frac{b_{mj}}{(m+1) f_{pj}^{m+1}(z)}, & z \in \mathscr{D}_j^p, \\ \sum_{m=2}^{M_{pj}} \frac{b_{-mj}}{m-1} f_{pj}^{m-1}(z), & z \notin \mathscr{D}_j^p, \end{cases} \tag{A.2}$$

$$\varphi_j^h(z) = \eta \sum_{m=1}^{M_{hj}} c_{-mj} f_{hj}^m(z), \tag{A.3}$$

$$\begin{aligned} \psi^{(\mathrm{o})}(z) = -\eta \Bigg\{ & \sum_{m=1}^{M_\mathrm{o}} \frac{\overline{c}_{-m\mathrm{o}}}{f_\mathrm{o}^m(z)} + c_{1\mathrm{o}} \frac{\overline{z}_\mathrm{o}}{R_\mathrm{o}} + \left(1 + \frac{\overline{z}_\mathrm{o}}{R_\mathrm{o} f_\mathrm{o}(z)}\right) \sum_{m=2}^{M_\mathrm{o}} m \frac{c_{m\mathrm{o}}}{f_\mathrm{o}^{m-2}(z)} \\ & + \frac{R_\mathrm{o}}{2\mu_\mathrm{m}} \left[\kappa_\mathrm{m} \sum_{m=2}^{M_\mathrm{o}} \frac{\overline{b}_{-m\mathrm{o}}}{(m-1) f_\mathrm{o}^{m-1}(z)} + b_{0\mathrm{o}} \frac{\overline{z}_\mathrm{o}}{R_\mathrm{o}} + \left(1 + \frac{\overline{z}_\mathrm{o}}{R_\mathrm{o} f_\mathrm{o}(z)}\right) \sum_{m=1}^{M_\mathrm{o}} \frac{b_{m\mathrm{o}}}{f_\mathrm{o}^{m-1}(z)} \right] \Bigg\}, \end{aligned} \tag{A.4}$$

$$\psi_j^p(z) = \eta R_j^p \times \begin{cases} (a_{1j} - a_{3j}) \sum_{m=2}^{M_{pj}} \frac{\overline{b}_{-mj}}{(m-1) f_{pj}^{m-1}(z)} \\ \quad - a_{1j} \left[b_{0j} \frac{\overline{z}_j^p}{R_j^p} + \left(\frac{\overline{z}_j^p}{R_j^p} + f_{pj}(z) \right) \sum_{m=1}^{M_{pj}} \frac{b_{mj}}{f_{pj}^m(z)} \right], & z \in \mathscr{D}_j^p, \\ a_{1j} \left(\frac{\overline{z}_j^p}{R_j^p} + f_{pj}(z) \right) \sum_{m=2}^{M_{pj}} b_{-mj} f_{pj}^m(z) + (2a_{1j} - a_{3j}) b_{0j} f_{pj}(z) \\ \quad + (a_{1j} - a_{3j}) \sum_{m=1}^{M_{pj}} \frac{\overline{b}_{mj}}{m+1} f_{pj}^{m+1}(z), & z \notin \mathscr{D}_j^p, \end{cases} \tag{A.5}$$

$$\psi_j^h(z) = \eta \left\{ \left(\frac{\overline{z}_j^h}{R_j^h} + f_{hj}(z) \right) \sum_{m=1}^{M_{hj}} m c_{-mj} f_{hj}^{m+1}(z) - 2\mathrm{Re}(c_{1j}) f_{hj}(z) - \sum_{m=2}^{M_{hj}} \overline{c}_{mj} f_{hj}^m(z) - \lambda_\mathrm{m} p_j R_j^h f_{hj}(z) \right\}, \tag{A.6}$$

where η is defined as in (4) and $\lambda_\mathrm{m} = (1-\kappa_\mathrm{m})/(2\mu_\mathrm{m})$.

Appendix B. Modification of the expressions for potentials

In the modified embedding method, $\varphi^{(o)}(z)$ and $\psi^{(o)}(z)$ expressed in (A.1) and (A.4) can be reduced to

$$\varphi^{(o)}(z) = \eta R_o \sum_{m=0}^{M_o} \frac{q_m}{(m+1) f_o^{m+1}(z)}, \tag{B.1}$$

$$\psi^{(o)}(z) = -\eta R_o \left\{ \sum_{m=1}^{M_o} \frac{\overline{q}_{-m}}{m f_o^m(z)} + q_o \frac{\overline{z}_o}{R_o} + \left(1 + \frac{\overline{z}_o}{R_o f_o(z)}\right) \sum_{m=1}^{M_o} \frac{q_m}{f_o^{m-1}(z)} \right\}. \tag{B.2}$$

References

Barnes, R.J., Janković, I., 1999. Two-dimensional flow through large number of circular inhomogeneities. Journal of Hydrology 226, 204–210.

Boley, B.A., 1961. A method of heat conduction analysis of melting and solidification problems. Journal of Mathematical Physics 40, 300–313.

Boley, B.A., Yagoda, H.P., 1971. The three-dimensional starting solution for a melting slab. Proceedings of the Royal Society of London A 323, 89–110.

Chen, K.T., Ting, K., Yang, W.S., 2000. Stress analysis of two-dimensional perforated plates using boundary element alternating method. Computers & Structures 75, 515–527.

Crouch, S.L., Mogilevskaya, S.G., 2003. On the use of Somigliana's formula and Fourier series for elasticity problems with circular boundaries. International Journal for Numerical Methods in Engineering 58, 537–578.

Eischen, J.W., Torquato, S., 1993. Determining elastic behavior of composites by the boundary element method. Journal of Applied Physics 74, 159–170.

Golub, G.H., Van Loan, C.F., 1996. Matrix Computations, third ed. John Hopkins University, Baltimore.

Greengard, L., Helsing, J., 1998. On the numerical evaluation of elastostatic fields in locally isotropic two-dimensional composites. Journal of the Mechanics and Physics of Solids 46, 1441–1462.

Helsing, J., Jonsson, A., 2002. Stress calculations on multiply connected domains. Journal of Computational Physics 176, 456–482.

Isida, M., Sato, R., 1984. Analysis of finite regions containing a circular hole or inclusion with application to their periodic arrays. Transactions of the Japan Society of Mechanical Engineers A 50, 1619–1627.

Kong, F., Yao, Z., Zheng, X., 2002. BEM for simulation of a 2D elastic body with randomly distributed circular inclusions. Acta Mechanica Solida Sinica 15, 81–88.

Linkov, A.M., 1983. Plane problems of the static loading of a piecewise homogeneous linearly elastic medium. Journal of Applied Mathematics and Mechanics 47, 527–532.

Linkov, A.M., Mogilevskaya, S.G., 1994. Complex hypersingular integrals and integral equations in plane elasticity. Acta Mechanica 105, 189–205.

Linkov, A.M., Mogilevskaya, S.G., 1998. Complex hypersingular BEM in plane elasticity problems. In: Sladek, V., Sladek, J. (Eds.), Singular Integrals in Boundary Element Methods. Computational Mechanics Publication, Southhampton (Chapter 9).

Liu, Y.J., Xu, N., Luo, J.F., 2000. Modeling of interphases in fiber-reinforced composites under transverse loading using the boundary element method. Journal of Applied Mechanics 67, 143–150.

Meguid, S.A., 1986. Finite element analysis of defense holes systems for the reduction of stress concentration in a uniaxially loaded plate with two coaxial holes. Engineering Fracture Mechanics 25, 403–413.

Mogilevskaya, S.G., Crouch, S.L., 2001. A Galerkin boundary integral method for multiple circular elastic inclusions. International Journal for Numerical Methods in Engineering 52, 1069–1106.

Mogilevskaya, S.G., Crouch, S.L., 2002. A Galerkin boundary integral method for multiple circular elastic inclusions with homogeneously imperfect interfaces. International Journal of Solids and Structures 39, 4723–4746.

Mogilevskaya, S.G., Crouch, S.L., 2004. A Galerkin boundary integral method for multiple circular elastic inclusions with uniform interphase layers. International Journal of Solids and Structures 41, 1285–1311.

Muskhelishvili, N.I., 1963. Some Basic Problems of the Mathematical Theory of Elasticity. Noordhoff, Groningen.

Wacker, G., Bledzki, A.K., Chate, A., 1998. Effect of interphase on the transverse Young's modulus of glass/epoxy composites. Composites A 29, 619–626.

Wang, J., Andreasen, J.H., Karihaloo, B.L., 2000. The solution of an inhomogeneity in a finite plane region and its application to composite materials. Composites Science and Technology 60, 75–82.

Wang, J., Mogilevskaya, S.G., Crouch, S.L., 2001. A Galerkin boundary integral method for nonhomogeneous materials with cracks. In: Elsworth, D., Tinucci, J., Heasley, K. (Eds.), Rock Mechanics in the National Interest. AA Balkema, Lisse, pp. 1453–1460.

Wang, J., Crouch, S.L., Mogilevskaya, S.G., 2003a. A complex boundary integral method for multiple circular holes in an infinite plane. Engineering Analysis with Boundary Elements 27, 789–802.

Wang, J., Mogilevskaya, S.G., Crouch, S.L., 2003b. Benchmarks results for the problem of interaction between a crack and a circular inclusion. Journal of Applied Mechanics 70, 619–621.

Wang, J., Mogilevskaya, S.G., Crouch, S.L., 2003c. A numerical procedure for multiple circular holes and elastic inclusions in a finite domain with a circular boundary. Computational Mechanics 32, 250–258.

Wang, J., 2004. Numerical modeling of elastic materials with inclusions, holes, and cracks. PhD thesis, University of Minnesota.

Wang, J., Crouch, S.L., Mogilevskaya, S.G. A fast and accurate algorithm for a Galerkin boundary integral method. Computational Mechanics, in press.

Woo, C.W., Chan, W.S., 1992. Boundary collocation method for analyzing perforated plate problems. Engineering Fracture Mechanics 43, 757–768.